

Implementation of new software for fast screening of cell compatibility on surface modifications using low-contrast time-lapsed microscopy

Dan Dominik Brüllmann · Marc O. Klein ·
Bilal Al-Nawas · Sigrid Horn · Verena Büsser ·
Barbara Jung · Wilfried Wagner · Bernd d'Hoedt

Received: 29 June 2009 / Accepted: 7 August 2009 / Published online: 21 August 2009
© Springer-Verlag 2009

Abstract Assessment of cell adhesion and cell size provides valuable information on surface biocompatibility. However, most investigations on cell morphology dynamics are time and resource consuming, of rather descriptive character and lack procedures for appropriate quantification. The aim of the study was to develop a software programme which allows automated cell segmentation and identification as well as calculation and further processing of cell size in low-contrast images. The software utilises modified edge detection and morphologic operations for automatic cell analysis in light microscopy images. In an application study, osteogenic cell-adhesion dynamics were quantified for the ECM proteins collagen type I (COL) and fibronectin (FIB) over a period of 12 hrs. Untreated tissue culture polystyrene (TCPS) served as control. The software programme proofed full function in automatic cell tracking and quantification of cell size. After 11 h, cell sizes were

highest for COL ($6391 \pm 1167 \mu\text{m}^2$) and FIB ($6036 \pm 411 \mu\text{m}^2$) compared with TCPS ($3261 \pm 693 \mu\text{m}^2$). The developed software allows quantification of initial cell size changes on translucent surface modifications and is suitable as a reliable tool for fast biocompatibility screening. Osteogenic cell adhesion was significantly promoted by COL and FIB indicating the potential of respective functionalized biomaterial surfaces.

Keywords Live cell imaging · Automatic segmentation · Cell-adhesion dynamics · Biocompatibility

Introduction

Early cell–substrate interactions play a pivotal role for many physiological and pathophysiological processes.

D. D. Brüllmann (✉) · B. d'Hoedt
Department of Oral Surgery,
University Medical Center of the Johannes Gutenberg University
Mainz,
Augustusplatz 2,
55131 Mainz, Germany
e-mail: bruellmd@mail.uni-mainz.de

M. O. Klein · B. Al-Nawas · V. Büsser · W. Wagner
Department of Oral and Maxillofacial Surgery,
University Medical Center of the Johannes Gutenberg University
Mainz,
Augustusplatz 2,
55131 Mainz, Germany

M. O. Klein
e-mail: klein@mkg.klinik.uni-mainz.de

B. Al-Nawas
e-mail: al-nawas@mkg.klinik.uni-mainz.de

V. Büsser
e-mail: VerenaBuesser@gmx.de

W. Wagner
e-mail: wagner@mkg.klinik.uni-mainz.de

S. Horn
Department of Neurosurgery,
University Medical Center of the Johannes Gutenberg University
Mainz,
Langenbeckstraße 1,
55131 Mainz, Germany
e-mail: shorn@uni-mainz.de

B. Jung
Department of Physics, Mathematics and Computer Science,
Johannes Gutenberg-University Mainz,
Staudingerweg 9,
55099 Mainz, Germany
e-mail: beijung@web.de

These interactions frequently result in characteristic cell adhesion dynamics and changes of the cellular phenotype [1, 2]. As an implication, capturing of cell-adhesion dynamics with resulting cell morphology might be utilised to identify promising substrate properties of high biocompatibility. High-throughput content screening using cell image-based assays offers a powerful new tool for understanding the biology of initial cellular adhesion dynamics [3–5]. Image-based live-cell assay experiments need to generate and analyse a large amount of images collected over a short period of time using automated high microscopy data acquisition. Since thousands of cells typically are needed to be screened for respective cell experiments, fast and highly reliable image analysis algorithms are of critical importance even in low-contrast images. One fundamental task of automated screening systems is accurate cell segmentation that often precedes other analyses such as cell morphology, tracking and dynamic behaviour. The accurate and computationally efficient segmentation of cells without distinct edges which become more indistinct at the start of adhesion is the focus of this paper.

In modern regenerative dentistry and dental implantology, various biomaterials with specific surface properties like bone substitute materials, occlusive membranes or dental implants have been introduced and are in the focus of ongoing research activities. For the incorporation and osseointegration of the applied biomaterial, adequate responses of adjacent cell populations are indispensable. For example, during peri-implant healing, mechanisms of new bone formation require the active migration of osteogenic cells to the implant surface with subsequent controlled adhesion at the surface. Successful and timely cell attachment is obligate precondition for further cell proliferation and differentiation. Fast and plane cell adhesions are attributes of biocompatible surfaces. Furthermore, various studies showed that these “biologically active” surfaces are closely associated with characteristic cell morphologies. Osteogenic cells cultivated on biocompatible surfaces represented a stretched, spindle-shaped phenotype with development of lamellipodias and filopodias, whereas less compatible surfaces resulted in rather roundish cell forms [6–9].

It is well accepted that extracellular matrix (ECM) components like collagen and fibronectin play a regulatory role for osteogenic cell functions and specifically promote osteogenic cell adhesion or motility [10–14]. Furthermore, over the actin-supported signalling pathway between extracellular matrix and intracellular compartments, the outside–in signalling for proliferation and cellular differentiation is regulated [15]. The aim of the study was to develop a programme which allows automated cell identification with quantification of cell surface and motility

parameters. In an application study, osteogenic cell adhesion dynamics were quantified for the ECM proteins collagen type I and fibronectin over a period of 12 hrs.

Materials and methods

Cell culture and substrates

A commercial hipbone-derived osteogenic cell line (HHOBc, PromoCell, Heidelberg, Germany) was utilised. Cells were cultivated using standard osteoblast cultivation medium, consisting of foetal calf serum (FCS, Gibco Invitrogen, Karlsruhe, Germany), Dulbecco's modified Eagle's medium (DMEM, Gibco Invitrogen), dexamethasone (100 nmol/l, Serva Bioproducts, Heidelberg, Germany), L-glutamin (Gibco Invitrogen) and streptomycin (100 mg/ml, Gibco Invitrogen). Cultivation was carried out at 37°C in a constant humidified atmosphere of 95% air and 5% CO₂.

Before our investigations, the cell line was qualitatively characterised by immunohistochemical expression of alkaline phosphatase (AP) and osteocalcin (labelled streptavidin–biotin/horseradish peroxidase). Cells were passaged at regular intervals depending on their growth characteristics using 0.25% trypsin (Seromed Biochrom KG, Berlin, Germany). All trials were taken out at the 5th cell passage. Osteogenic cells were detached and seeded on the different test substrates (see following) with a concentration of $1 \cdot 10^4$ cells /ml. As representatives of solitaire ECM-proteins, collagen type I (human placenta; Sigma, St.Louis, USA) and fibronectin (human foreskin fibroblasts; Sigma, St. Louis, USA) were utilised. The lyophilized powders were dissolved in PBS supplemented with 1 mmol CaCl₂ and adjusted to a concentration of 100 µg/ml. petri dishes (tissue culture polystyrene (TCPS); Greiner Holding AG, Kremsmuenster, Austria) were incubated with 2,000 µl of the respective working solutions for 1 h at 37°C, thus allowing the proteins to precipitate on the TCPS surface. Soluble remnants were removed by rinsing gently with PBS. Potential remaining free adhesion sites were blocked with a solution of 1% BSA for 30 minutes at room temperature. Untreated TCPS served as control.

Images were acquired on an inverse phase–contrast microscope (Nikon Diaphot-TMD, Nikon, Düsseldorf, Germany) equipped with a Styrofoam-isolated lucite cube enclosing the stage. Haemostasis inside the incubation cube was provided by a heating coil, a thermostat, temperature sensors (Heraeus, Hanau, Germany; Shiley, Irvine, CA, USA), a mini-fan, a CO₂ insufflation system and a CO₂-regulation unit (Heraeus). Immediately after incubation with osteogenic cells, the respective test substrates (collagen type I, fibronectin, TCPS-control) were placed into the

controlled-atmosphere lucite box, and randomly selected areas were observed for a period of 12 h. Images were recorded with a CCD camera (The ImagingSource DFK 41BF02, The ImagingSource Europe GmbH, Bremen, Germany) and stored as uncompressed bitmaps. Images were captured every 60 min with the supplied software (IC Capture, The ImagingSource Europe GmbH, Bremen, Germany) and a resolution of 640×480 pixels. For each test substrate, three consecutive assays were performed. Altogether, we analysed 20 cells cultivated on collagen type I, 25 cells cultivated on fibronectin and 23 cells cultivated on TCPS.

Image segmentation algorithm

The flowchart of the used algorithm shown in Fig. 1 comprises six stages: First a background correction is conducted using a modified unsharp masking technique [16, 17]. A background image B is estimated through a median filtered image. The output of the median filter with input samples, $x_1, x_2, \dots, x_N, N = 2k + 1$, is the $k+1$ 'th smallest value of the set $\{x_1, x_2, \dots, x_N\}$. Once subtracted from the original image I, it generates the result image with equalised illumination R,

$$R(x, y) = 128 + I(x, y) - B(x, y) \tag{1}$$

In a next step, an edge image is created calculating the gradient magnitude by discrete convolution of the image with sobel masks [17–21] in x- and y-direction. This image containing the objects' edge magnitude (See Fig. 2a) is further binarized by a histogram-based threshold algorithm introduced by Zack in 1977 [22]. The function $h_{(i)}, i \in [0..255]$, is the histogram of pixel intensities. A line l was

fitted to this histogram using the start point $A(0, h_{(0)})$ and $B(x, h_{(x)})$, where x denotes the location of the histogram maximum. A third point has to be searched by the software for thresholding purposes by determining a third point $C(y, h_{(y)})$ which is located in a maximum distance to l . The equation for a straight line between A and B is calculated by its slope:

$$m = \frac{h_{(x)} - h_{(0)}}{x} \tag{2}$$

Using slope m , the distance d between l and $h_{(j)}, j \in [0..x]$ can be calculated as

$$d = \left| \frac{(m \cdot j - h_{(j)} + h_{(0)})}{\sqrt{m^2 + 1}} \right| \tag{3}$$

in order to find the biggest distance d_{max} between line and histogram. Thus, a global search threshold t can be added by adding a fixed offset chosen by the user to d_{max} (See Fig. 2b).

The binary image $B(x, y)$ is then created as:

$$B(x, y) = \begin{cases} 0 & \text{if } R(x, y) < d_{max} + \text{offset} \\ 1 & \text{else} \end{cases} \tag{4}$$

Then, small objects are removed from the binarized image (See Fig. 2c). In a further step, objects are closed (See Fig. 2d) by creating an image $F(x, y)$ where black background pixels outside the objects are set to white using a floodfill algorithm [23] to create the cleaned image $C(x, y)$ using a XNOR operation:

$$C(x, y) = f(B, F) = B \bullet F + \overline{B + F} \tag{5}$$

The objects are saved using labelling operations [17, 19, 24]. For the following, we assume the binary input image $C(x, y)$ copied to a two-dimensional array of integers where objects are set to 1 and background to 0. The labelling operator scans the array by moving along a row until it comes to a point p (where p denotes the pixel to be labelled) for which $L(x, y) = n$. When this is true, it examines recursively the four neighbours in edge to edge connectivity of p and changes the neighbouring pixels to the current object number n (See Fig. 2e), similar to a floodfill algorithm [23].

$$L(x, y) = \begin{cases} 0 \\ 1 \\ n \in 2, 3, \dots \end{cases} \tag{6}$$

Thus, saved objects can be extracted from the label image $L(x, y)$ and be saved into Excel (Excel, Microsoft) tables according to user predefined geometrical parameters like minimal size, maximal size and roundness.

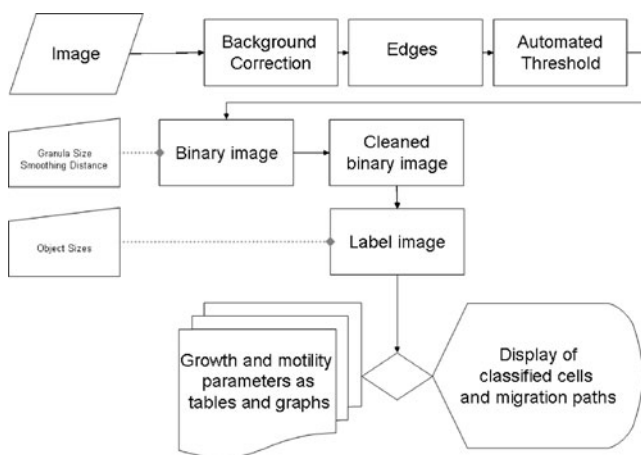


Fig. 1 Flowchart of the algorithm used. The solid arrows indicate data process flow. Dotted lines illustrate settings predefined by the user

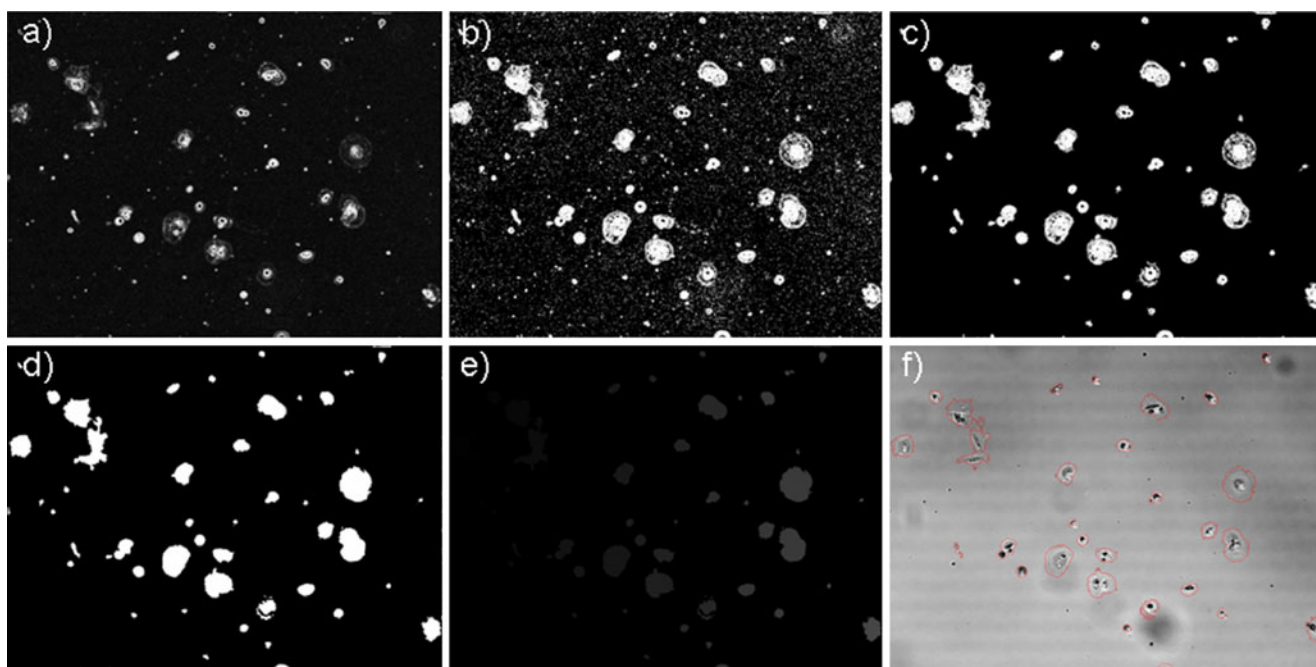


Fig. 2 Edge magnitude image (a) and the resulting binarized image (b), and it's cleaned derivative (c). Objects were closed using flood fill and xnor operations (d) in order to prepare image for labelling (e).

Cell boundaries are outlined by *red edges* superimposed to the original image (f)

Results

Implementation and software

The cell tracking software was implemented using Borlands Delphi 7 IDE (Borland, Langen, Germany). The software is able to detect cells in low-contrast images according to the described techniques. The performance of the proposed algorithm was measured on a Sony Vaio VGN-SZ2XO/C laptop computer with a 2 GHz Dual-Core CPU and 1 GB of main memory under the operating system of Microsoft Windows XP Professional. The total computation time averages about 1.67 s for 320×240 -sized images containing between six to eight cells (minimum computation time 1.62 s, maximum computation time 1.72 s). For images the size of 640×480 pixels containing between ten and 13 cells, we found an average computation time of 6.45 s (minimum computation time 6.42 s, maximum computation time 6.47 s), and for images the size of 1280×960 pixels containing between ten and 13 cells, we found an average computation time of 17.34 s (minimum computation time 17.19 s, maximum computation time 17.61 s). Performance tests showed that computation time depends on the size of the input images on one hand and the number of observed cells on the other (see Fig. 3).

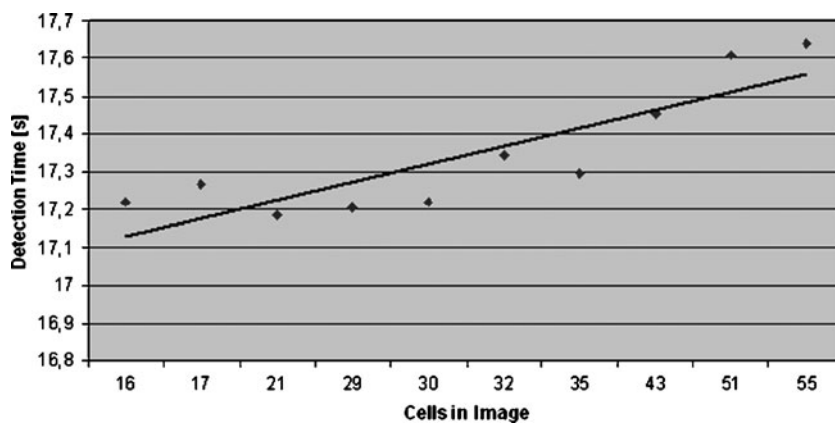
The described software is able to detect cells in low-contrast images. The user can predefine threshold offsets, size of removed noise or granulae (caused by vitiations in culture media) and closing of objects. Because acquisition

time of an image is stored in the header of a bitmap by commercial capture software delivered with the cameras (i.e. IC Capture, The ImagingSource Europe GmbH, Bremen, Germany), the software described in this article is able to extract this information to save it together with the number of detected cells, the size of their area in micrometers, their circumference and their roundness into Excel tables to describe cell growth and motility parameters (See Fig. 4). The tables are used to calculate graphs of the growth of all cells or a special selected single cell. Additionally, motility paths can be calculated and displayed on the current cell image.

Osteogenic cell-adhesion studies

The investigated substrates resulted in different cell adhesion dynamics as well as in different cell sizes. For all three surfaces, initial cell sizes of the still-detached cells at 0 hrs were basically in the same dimension, ranging from $904 \pm 30 \mu\text{m}^2$ for fibronectin (FIB) to $1284 \pm 75 \mu\text{m}^2$ for collagen type I (COL). For all other time points, values for TCPS were significantly lowest with a maximum of $3261 \pm 693 \mu\text{m}^2$ after 11 hrs. Values for COL and FIB showed no significant difference to each other and indicated a fast and stronger increase of cell size exceeding the TCPS maximum already after 3 hrs (COL, $3717 \pm 684 \mu\text{m}^2$, FIB: $3649 \pm 522 \mu\text{m}^2$). Maximum values were $6391 \pm 1167 \mu\text{m}^2$ for COL and $6,036 \pm 411 \mu\text{m}^2$ for FIB after 11 hrs (See Fig. 5). In order to evaluate the

Fig. 3 Performance tests on images with a resolution of 1280×960 pixels showing the computation time depending on number of cells observed in the image



developed method for accurateness, we compared it with two popular existing methods. As illustrated in Fig. 6c, simple thresholding by an adaptive global threshold is not adequate because a darker cell (indicated by the red arrow) is missed. The images d, e, and f show that the tested canny edge detector [17, 21, 25] either overestimates (at a smoothing parameter of sigma=1.0) or underestimates edges found in the images (at a smoothing parameter of sigma=3.0). Even if adequate values are chosen for sigma, there are further edge-linking algorithms needed to compute useful results.

Discussion

Compared with traditional, rather descriptive cell observation studies, reliable quantification of important cell attributes like cell size offers additional information on cell–substrate interactions. Furthermore, assessment of changes of cell size over time can be utilised to monitor dynamic cell adhesion on various substrates. The aim of the study was to introduce a new analysis procedure for automated, simple and fast cell tracking and analysis in order to extract quantitative data characterising cell

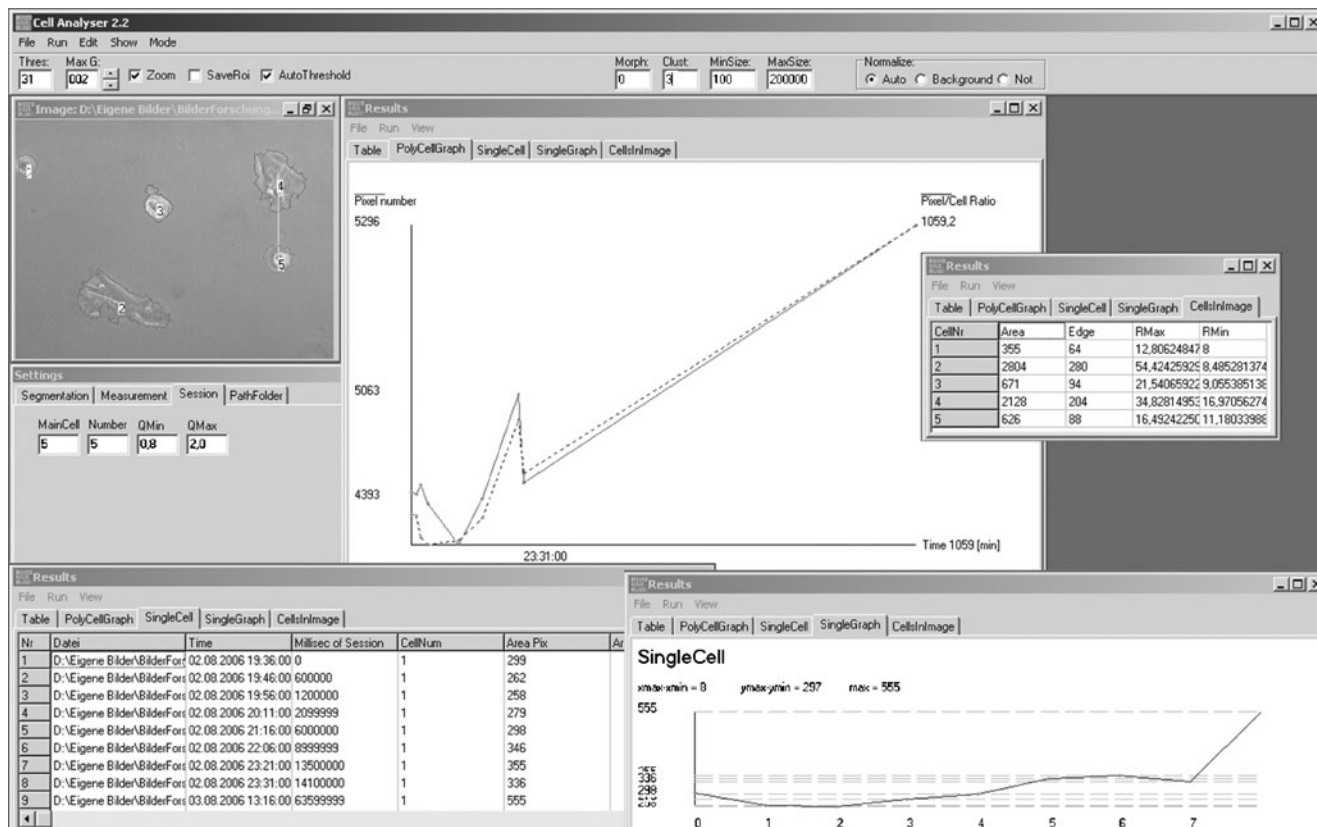
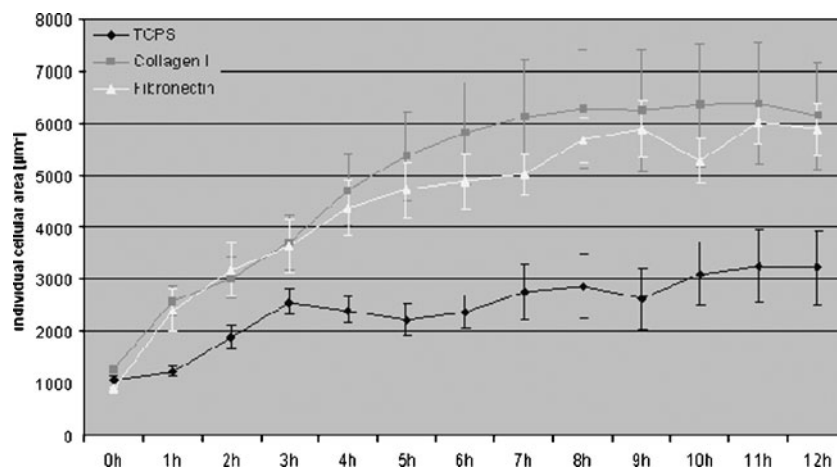


Fig. 4 Screenshot of the software described. Cells highlighted by red edges are superimposed by their individual migration paths (left). Cell growth is illustrated by curves and tables

Fig. 5 Mean values of cell size for the different investigated substrates. *Error bars* indicate standard deviations



responses to different substrates. Continuous in vitro cell imaging was achieved by live video microscopy coupled with automatic image analysis software. The employed light microscope allowed quick and easy observation and image acquisition, but the images were of low initial contrast which, additionally, could further worsen over observation time due to artefacts and focus changes. To cope with this problem, we implemented a simple, robust and fast segmentation algorithm composed of gradient operators and an adaptive threshold method. As shown before, see Fig. 6c, simple thresholding by an adaptive global threshold was not adequate because darker cells were missed. The tested canny edge detector either over-

estimates (at a smoothing parameter of $\sigma=1.0$) or underestimates edges found in the images (at a smoothing parameter of $\sigma=3.0$). Even if adequate σ values are selected for edge detection, there are further edge-linking algorithms needed to compute useful results. Thus, we decided to implement an unusual edge-detection method by applying an adaptive global threshold on a gradient image. As shown in Figs. 2f and 6b, the proposed method is adequate for low-contrast transmitted microscopy images. Similar systems for time-lapse video microscopy for automatic cell growth evaluation were described by Dallas et al., Debeir et al., Ersoy et al., Wang et al., Yue et al. and Zhang et al. [3–5, 26–28], whereas Debeir et al. reported a

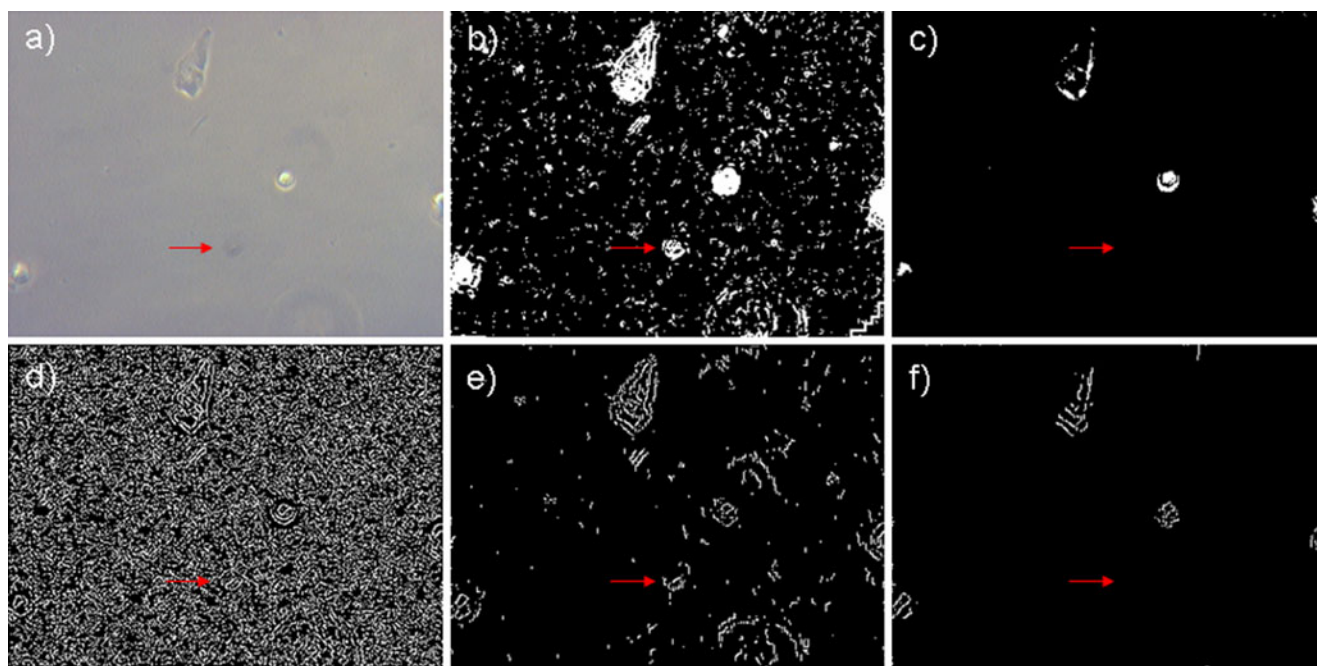


Fig. 6 Transmission light image (a) and resulting binary image of the edge detection described (b) without further cleaning of thresholding result. Simple thresholding by an adaptive global threshold is not adequate because a darker cell (indicated by the *red arrow*) is missed

(c). The images (d–f) show that the tested canny edge detector overestimates (at a smoothing parameter of $\sigma=1.0$) or underestimates edges found in the images (at a smoothing parameter of $\sigma=3.0$)

computation time of approximately 10 s for images of 700×500 pixels, which shows that our system is comparable fast. Our method can effectively segment grey scale images with poor background, such as that obtained from imaging cells cultured on substrate-coated tissue culture polystyrene (TCPS). The experimental results obtained using this method and comparisons with existing methods clearly show adequate function for fast and affordable screening test for functionalised surfaces by means of time-lapse light microscopy. We think that the method described can be easily adapted for other purposes. We think of the automated analysis of digital images of brush biopsies [29] or confocal laser scanning microscope images [30]. Investigation of surface-modified smooth TCPS, e.g. coated with functional ligands, serves as initial model for complex, non-translucent surface structures like titanium dental implants and provides first hints on biocompatibility of the surface modification. The results of our application study on modified TCPS surfaces indicated noticeable promotion of osteogenic cell adhesion dynamics and resulting cell size by the single ECM proteins collagen type I and fibronectin. As efficient cell adhesion is a mandatory precondition for further cell maturation, which additionally can be promoted by the investigated ECM ligands, our in vitro results are congruent with observed high performances of respectively functionalised dental implants in vivo [31–33]. As a summary, the developed software allows fast and uncomplicated quantification of initial cell reactions on (translucent) substrates and serves as a reliable tool for biocompatibility-screening of surface modifications.

Acknowledgements The authors would like to thank Monika Herr from the Department of Neurosurgery, University Hospital Mainz, Germany, for her excellent technical assistance during the whole project.

This project is supported by a grant from the German Association of Implantology (Deutsche Gesellschaft für Implantologie, DGI).

All authors disclose any actual or potential conflict of interest including any financial, personal or other relationships with other people or organisations within that could inappropriately influence this work.

References

- Bettinger CJ, Langer R, Borenstein JT (2009) Engineering substrate topography at the micro- and nanoscale to control cell function. *Angew Chem Int Ed Engl* 48(30):5406–5415
- Guilak F, Cohen DM, Estes BT, Gimble JM, Liedtke W, Chen CS (2009) Control of stem cell fate by physical interactions with the extracellular matrix. *Cell Stem Cell* 5(1):17–26
- Dallas SL, Veno PA, Rosser JL, Barragan-Adjemian C, Rowe DW, Kalajzi I, Bonewald LF (2009) Time lapse imaging techniques for comparison of mineralization dynamics in primary murine osteoblasts and the late osteoblast/early osteocyte-like cell line MLO-A5. *Cells Tissues Organs* 189:6–11
- Debeir O, Camby I, Kiss R, Van Ham P, Decaestecker C (2004) A model-based approach for automated in vitro cell Tracking and chemotaxis analyses. *Cytometry* 60(A):29–40
- Ersoy I, Palaniappan K (2008) Multi-feature contour evolution for automatic live cell segmentation in time lapse imagery. *Conf Proc IEEE Eng Med Biol Soc* 1:371–374
- El-Amin SF, Lu HH, Khan Y, Burems J, Mitchell J, Tuan RS, Laurencin CT (2003) Extracellular matrix production by human osteoblasts cultured on biodegradable polymers applicable for tissue engineering. *Biomaterials* 24(7):1213–1221
- Kim HJ, Kim SH, Kim MS, Lee EJ, Oh HG, Oh WM, Park SW, Kim WJ, Lee GJ, Choi NG et al (2005) Varying Ti-6Al-4 V surface roughness induces different early morphologic and molecular responses in MG63 osteoblast-like cells. *J Biomed Mater Res* 74(3):366–373
- Klein MO, Tapety F, Sandhöfer F et al (2006) Visualization of vital osteogenic cells on differently treated titanium surfaces using confocal laser scanning microscopy (CLSM)—a pilot study. *Z Zahnärztl Implantol* 21(4):145–153
- Park BS, Heo SJ, Kim CS, Oh JE, Kim JM, Lee G, Park WH, Chung CP, Min BM (2005) Effects of adhesion molecules on the behavior of osteoblast-like cells and normal human fibroblasts on different titanium surfaces. *J Biomed Mater Res A* 74:640–651
- Cooke MJ, Phillips SR, Shah DS, Athey D, Lakey JH, Przyborski SA (2008) Enhanced cell attachment using a novel cell culture surface presenting functional domains from extracellular matrix proteins. *Cytotechnology* 56(2):71–79
- Kirchhof K, Hristova K, Krasteva N, Altankov G, Groth T (2008) Multilayer coatings on biomaterials for control of MG-63 osteoblast adhesion and growth. *J Mater Sci Mater Med* 20(4):897–907
- Klein MO, Reichert C, Koch D, Horn S, Al-Nawas B (2007) In vitro assessment of motility and proliferation of human osteogenic cells on different isolated extracellular matrix components compared with enamel matrix derivative by continuous single-cell observation. *Clin Oral Implants Res* 18:40–45
- Liu G, Hu YY, Zhao JN, Wu SJ, Xiong Z, Lu R (2004) Effect of type I collagen on the adhesion, proliferation, and osteoblastic gene expression of bone marrow-derived mesenchymal stem cells. *Chin J Traumatol* 7(6):358–362
- Tsai WB, Ting YC, Yang JY, Lai JY, Liu HL (2009) Fibronectin modulates the morphology of osteoblast-like cells (MG-63) on nano-grooved substrates. *J Mater Sci Mater Med* 20(6):1367–1378
- Pienta KJ, Coffey DS (1992) Nuclear-cytoskeletal interactions: evidence for physical connections between the nucleus and cell periphery and their alteration by transformation. *J Cell Biochem* 49(4):357–365
- Polesel A, Ramponi G, Mathews VJ (2000) Image enhancement via adaptive unsharp masking. *IEEE Trans Image Process* 9(3):505–510
- Seul M, O’Gorman L, Sammon MJ (2005) Practical algorithms for image analysis, description, examples, and code. Cambridge University, Cambridge
- Davies ER (2005) Machine vision: theory algorithms practicalities. Elsevier, Heidelberg
- Gonzalez R, Woods R (1992) Digital image processing. Addison Wesley, Reading, MA
- Myler HR, Weeks AR (1993) Pocket handbook of image processing algorithms in C. Prentice Hall International, London, UK
- Parker JR (1999) Algorithms for image processing and computer vision. Wiley Computer Publishing, Wiley, New York
- Zack GW, Rogers WE, Latt SA (1977) Automatic measurement of sister chromatid exchange frequency. *J Histochem Cytochem* 25(7):741–753

23. Glassner A (1990) *Graphic gems*. Academic Press, Boston
24. Shi H (1995) Image algebra techniques for binary image component labeling with local operators. *J Math Imaging Vis* 5:159–170
25. Canny JF (1986) A computational approach to edge detection. *IEEE Trans Pattern Anal Mach Intell* 8:697–698
26. Wang M, Zhou X, Li F, Huckins J, King RW, Wong STC (2008) Novel cell segmentation and online SVM for cell cycle phase identification in automated microscopy. *Bioinformatics* 24(1):94–101
27. Yu D, Phama TD, Yan H, Zhang B, Crane DI (2007) Segmentation of cultured neurons using logical analysis of grey and distance difference. *J Neurosci Methods* 166:125–137
28. Zhang K, Xiong H, Zhou X, Yang L, Wang YL (2008) A confident scale-space shape representation framework for cell migration detection. *J Microsc* 231(3):395–401
29. Driemel O, Dahse R, Hakim SG, Tsioutsias T, Pistner H, Reichert TE, Kosmehl H (2007) Laminin-5 immunocytochemistry: a new tool for identifying dysplastic cells in oral brush biopsies. *Cytopathology* 18(6):348–355
30. Walter C, Klein MO, Pabst A, Al-Nawas B, Duschner H, Ziebart T (2009) Influence of bisphosphonates on endothelial cells, fibroblasts, and osteogenic cells. *Clin Oral Investig* Mar 18. [Epub ahead of print].
31. Schliephake H, Aref A, Scharnweber D, Bierbaum S, Sewing A (2009) Effect of modifications of dual acid-etched implant surfaces on peri-implant bone formation. Part I: organic coatings. *Clin Oral Impl Res* 20(1):31–37
32. Schliephake H, Scharnweber D, Dard M, Sewing A, Aref A, Roessler S (2005) Functionalization of dental implant surfaces using adhesion molecules. *J Biomed Mater Res B Appl Biomater* 73(1):88–96
33. Stadlinger B, Pilling E et al (2007) Influence of extracellular matrix coatings on implant stability and osseointegration: an animal study. *J Biomed Mater Res B Appl Biomater* 83(1):222–231

Copyright of Clinical Oral Investigations is the property of Springer Science & Business Media B.V. and its content may not be copied or emailed to multiple sites or posted to a listserv without the copyright holder's express written permission. However, users may print, download, or email articles for individual use.